Supporting Information for

Disentangling Oxygen and Water Vapor Effects on Optoelectronic Properties of Monolayer Tungsten Disulfide

*Hanyu Zhang[1], Jeremy R. Dunklin[1], Obadiah G. Reid[1,2], Seok Joon Yun[3], Sanjini U. Nanayakkara[1], Young Hee Lee[3,4], Jeffrey L. Blackburn[1], Elisa M. Miller[1]**

1. Materials and Chemical Science and Technology Directorate, National Renewable Energy Laboratory, 15013 Denver West Parkway, Golden, Colorado 80401, United States

2. Renewable and Sustainable Energy Institute, University of Colorado Boulder, Boulder, Colorado 80309, USA

3. Center for Integrated Nanostructure Physics (CINAP), Institute for Basic Science (IBS), Suwon, 16419 Republic of Korea

4. Department of Energy Science, Sungkyunkwan University, Suwon, 16419 Republic of Korea

Corresponding Authors

*Elisa.Miller@nrel.gov

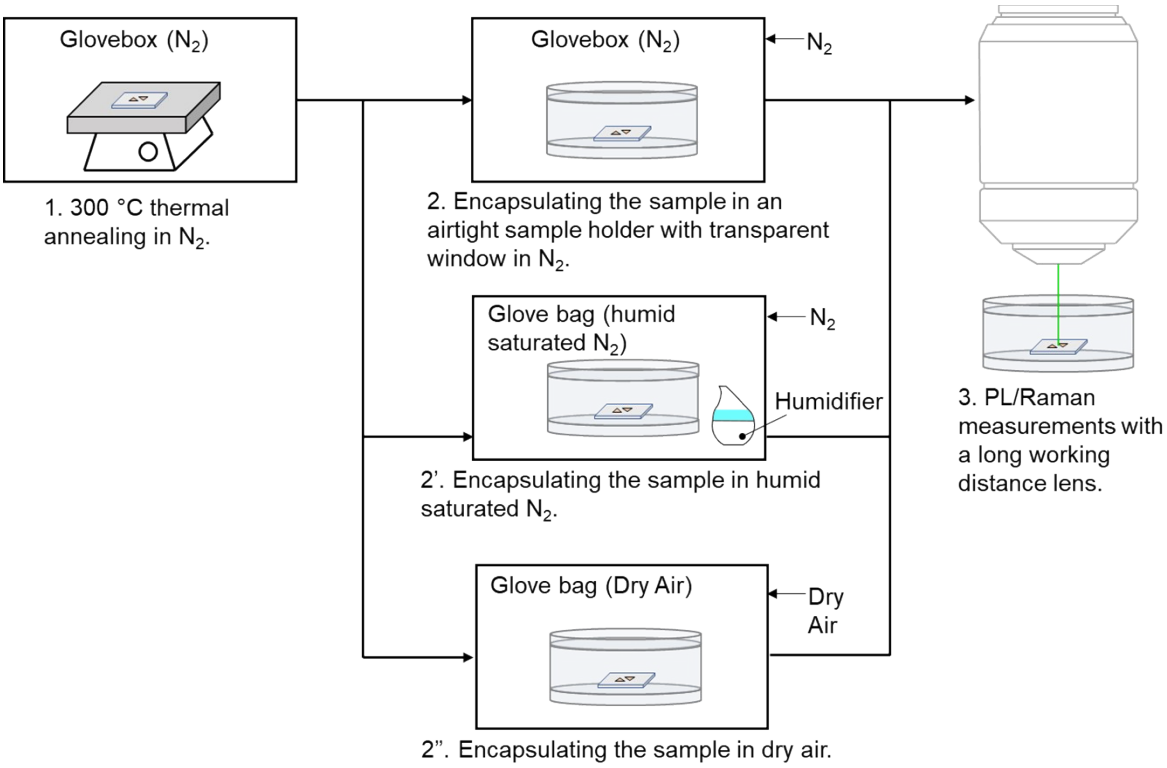

Schematic S1. Step 1: anneal the WS_2 monolayers at 300 °C in the glovebox with N_2 for 60 min. Step 2: encapsulate the WS_2 sample within the air-free sample holder in the N_2 glove box. Step 3: perform the optical measurements in controlled environments. Step 2': the humidity-controlled condition is created by a humidifier in a N_2 glove bag. Step 2": the glove gas is purged with dry air (~22% O_2 in N_2) to create the O_2 rich environment.

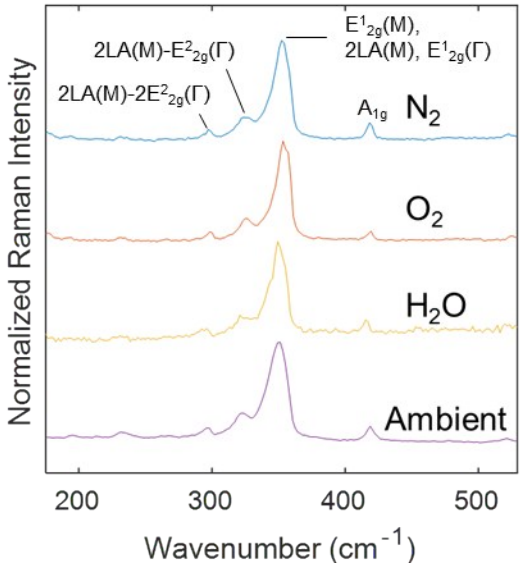

Figure S1. The Raman spectra of monolayer WS_2 in N_2, O_2, H_2O, and ambient condition with 119 μW of 532-nm laser illumination.

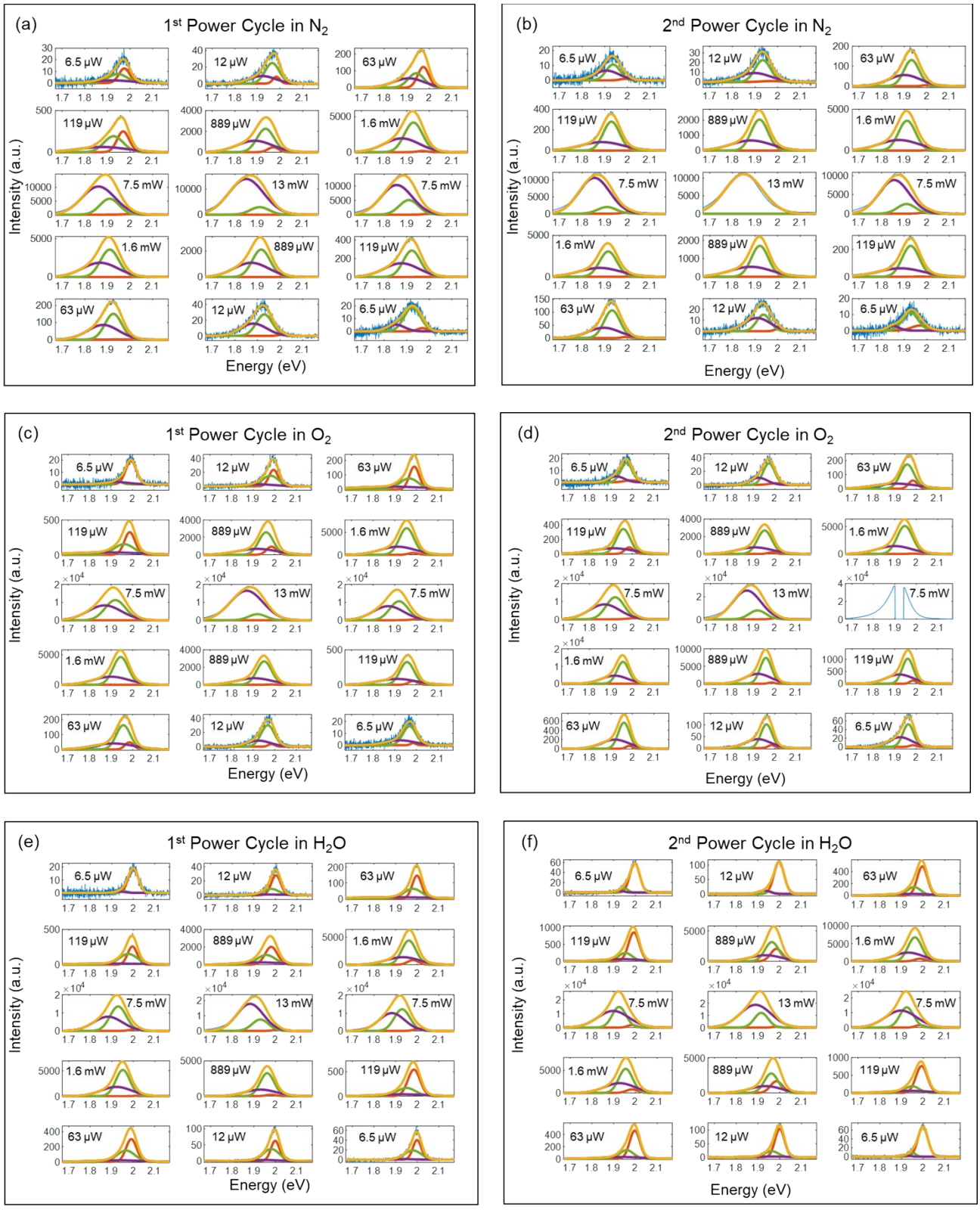

Figure S2. Monolayer WS_2 PL changes via (a, c, e) 1st and (b, d, f) 2nd laser power cycling of 532-nm laser irradiation under (a, b) N_2, (c, d) O_2, and (e, f) H_2O conditions. For each power cycle, the

excitation power increase from 6.5 μW to 12.9 mW and decrease back to 6.5 μW. The laser is focused on the same spot during the 1st and 2nd power cycles for each environment. The PL is decomposed into three Gaussian lineshapes (X^0 – red, X^- – green, LES – purple, sum − yellow) and are co-plotted with the raw PL (blue) data. The Gaussian centers are allowed to vary during the fitting in the range of 1.985-2.005 meV for X^0, 1.980-1.920 meV for X^-, and 1.87-1.935 meV for LES with minimum variances of 15 meV, respectively. The FWHM is plotted in Figure S4.

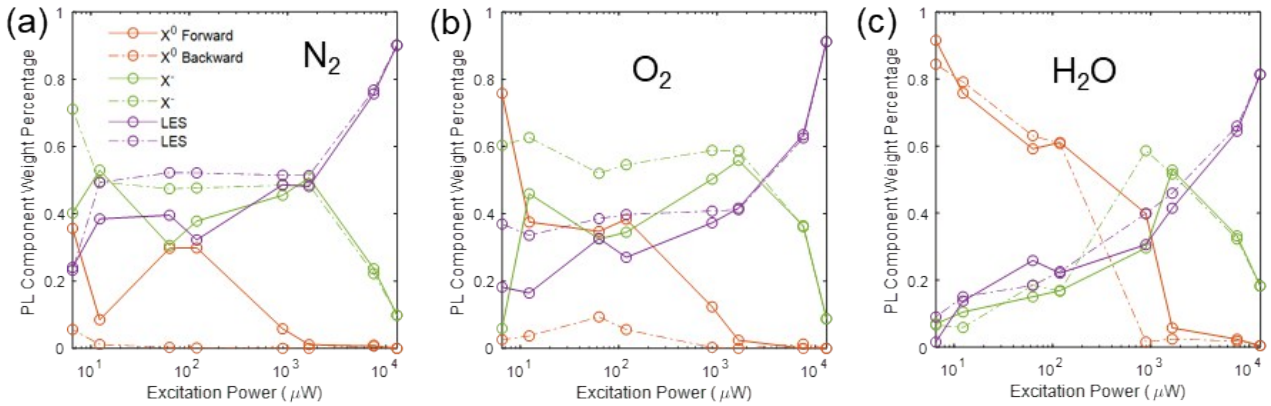

Figure S3. The integrated PL area percentages of the Gaussian components for X^0, X^-, and LES as a function of the excitation power from the 1st power cycle in Figure S2 for the (a) N_2 case, (b) O_2 case, and (c) H_2O case. The solid and dash lines represent excitation power ascending and descending, respectively.

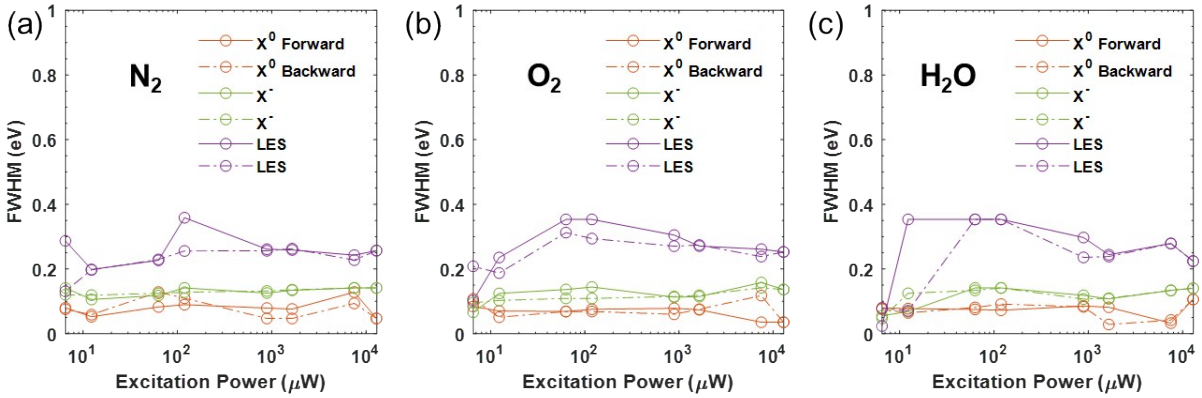

Figure S4. The FWHM of X^0, X^-, and LES from Figures 2 and S2 as a function of excitation power (a) in N_2, (b) O_2, and (c) H_2O for the first power cycle. Both the exciton and trion for all three cases remain consistent as the excitation power is increased and decreased. The LES has variation due to the nature of the LES combining multiple features, including biexciton and below-bandgap defect emission.

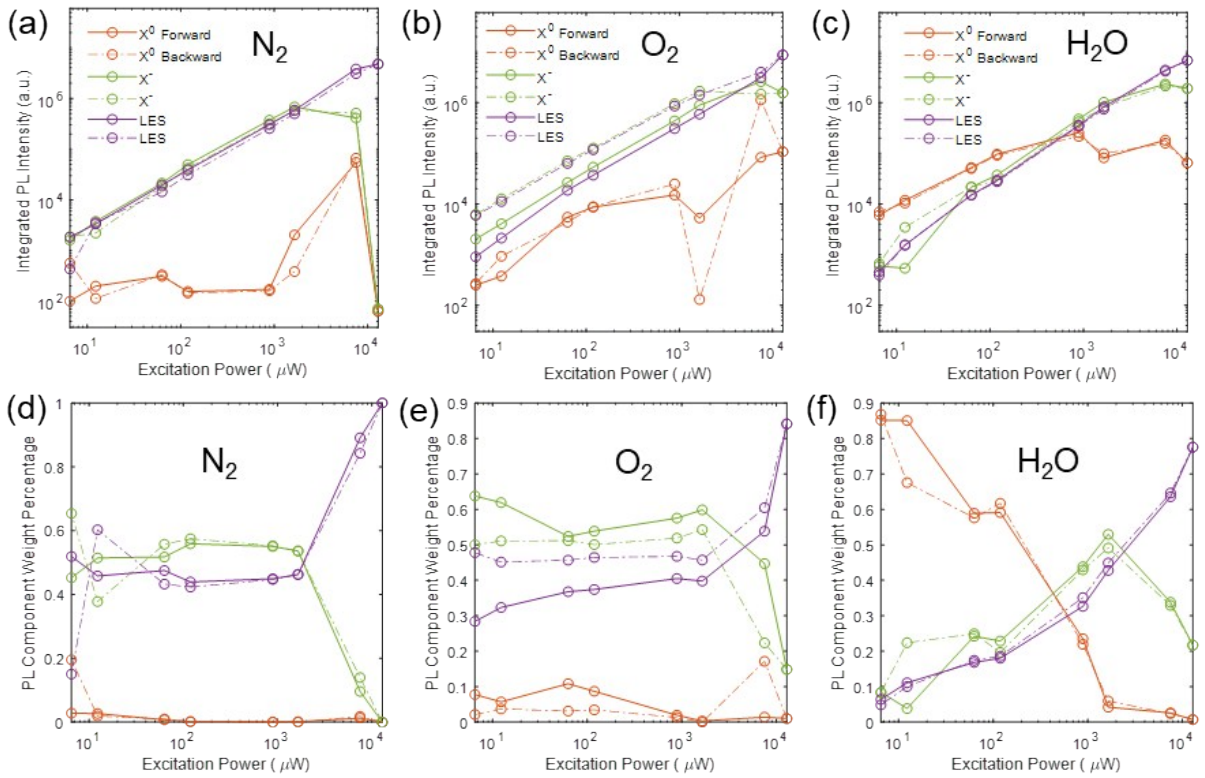

Figure S5. (Top) Integrated PL area from a Gaussian fit of X^0, X^-, and LES as a function of excitation power derived from the fitting results of the 2nd excitation power cycle from Figure S2b, d, and f for the three environments, (a) in N_2, (b) O_2, and (c) H_2O. (Bottom) Corresponding component percentages of the X^0, X^-, and LES in (d) N_2, (e) O_2, and (f) H_2O.

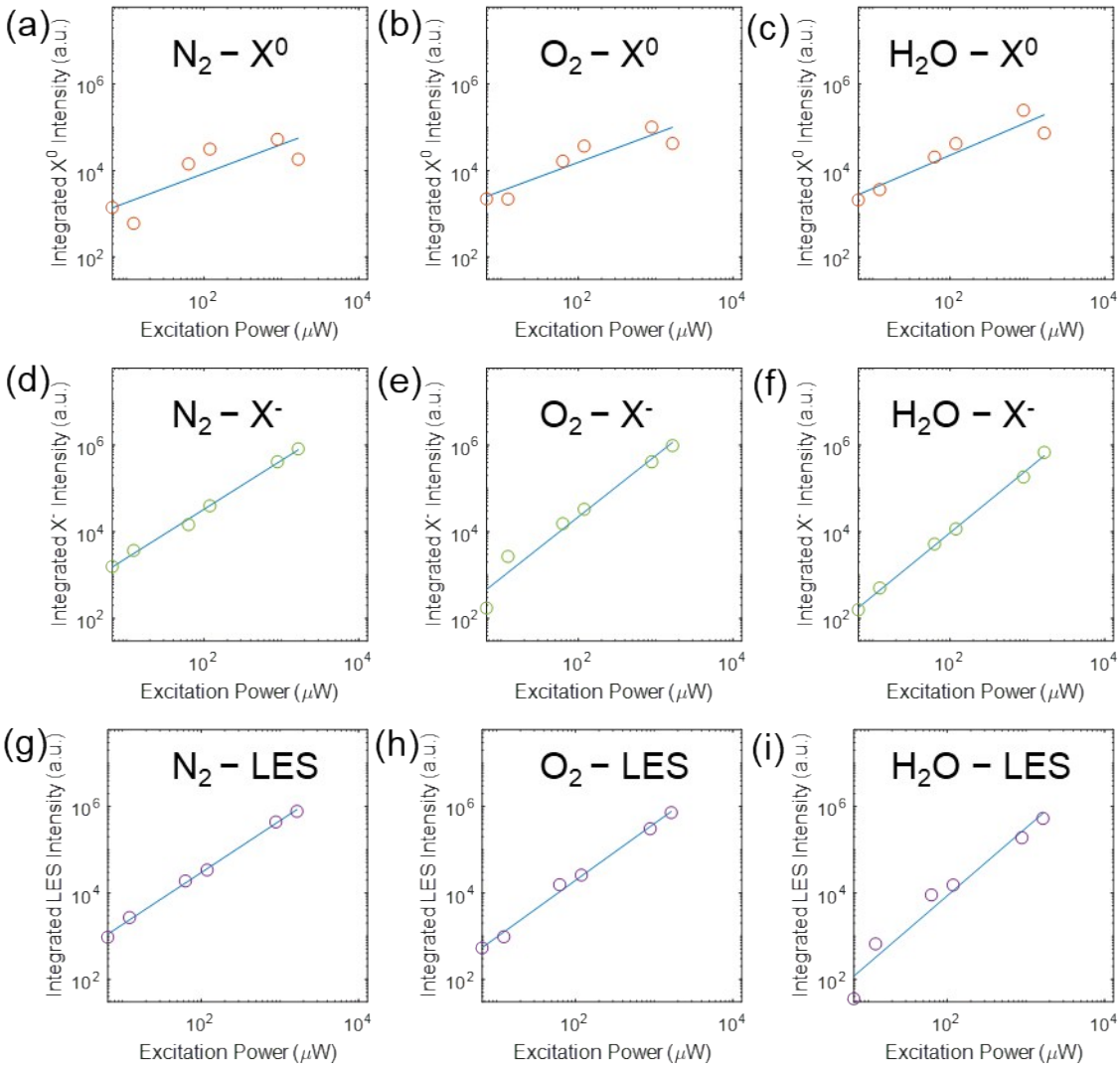

Figure S6. Linear fitting of the integrated PL area of Gaussian lineshapes for (a-c) X^0, (d-f) X^-, and (g-i) LES as a function of ascending excitation power for the first power cycle, where the data are extracted from the forward power cycle of Figure 3 for the three environments: (a, d, g) in N_2, (b, e, h) O_2, and (c, f, i) H_2O. Roughly similar results are obtained for each environment, in that the overall PL slope is m = 1.07, 1.11, and 1.10 for the N_2, O_2, and H_2O case, but there are slight differences when evaluating the induvial emission slopes (Table S1). A superlinear LES PL increase (m > 1) indicates the biexciton contribution to LES is significant as the laser power is increased because the biexciton has an expected power dependence that is about twice that of X^0.[1,2] This is to be expected that the population shifts to more multi-particle type emissions as the laser power increases; relatively, X^0 increasing is feeble and much less than X^- and LES. The individual fits and slopes for each type of emission are reported in Table S1.

Table S1. Extracted slopes from linear fits from Figure S6 for each PL contribution under various environments for ascending excitation power.

Round 1	N_2 (Forward)	O_2 (Forward)	H_2O (Forward)
X^0	0.65	0.64	0.74
X^-	1.09	1.36	1.41
LES	1.16	1.27	1.52
Overall	1.07	1.11	1.10

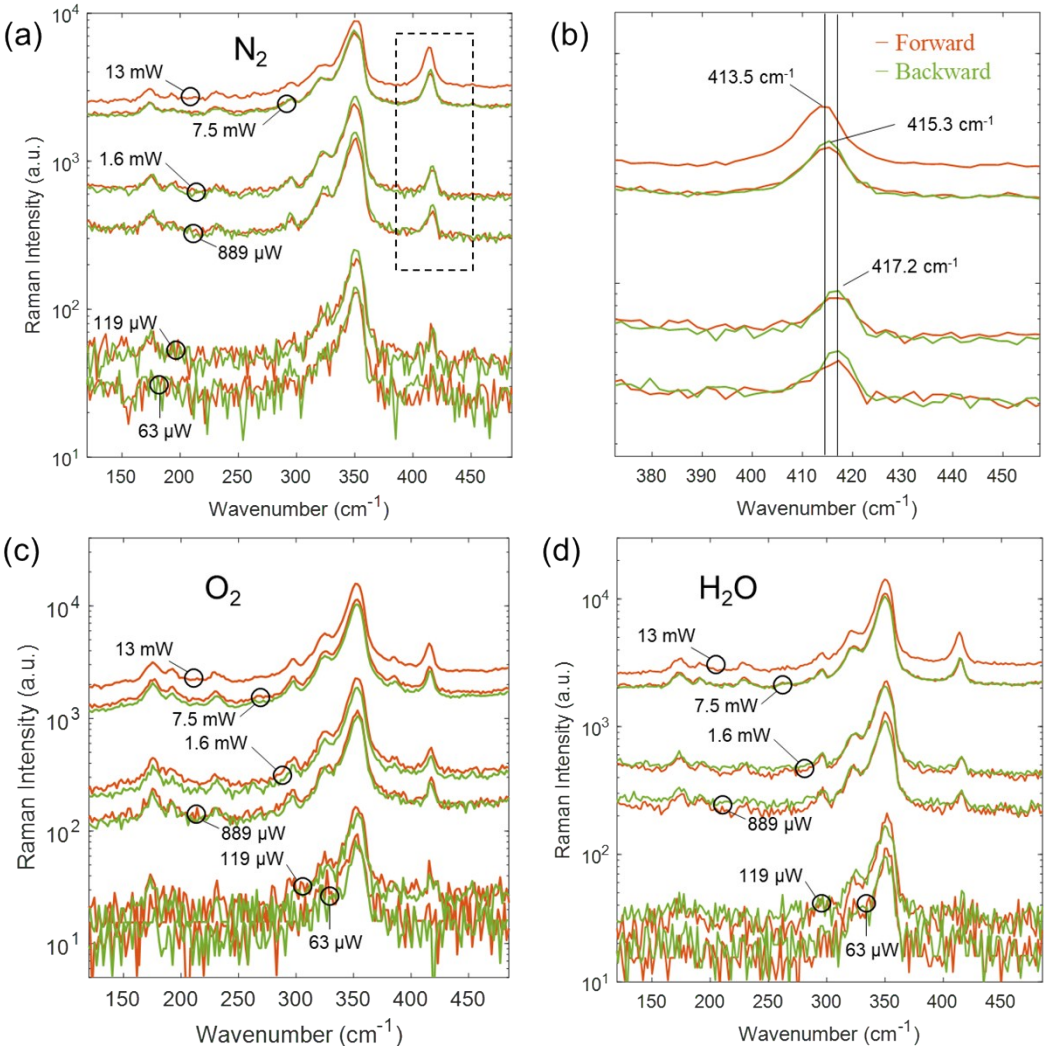

Figure S7. Raman spectral changes of the monolayer WS_2 from the laser power cycling of 532-nm laser irradiation under (a-b) N_2, (c) O_2, and (d) H_2O environments. The orange lines represent the power ascending while the green lines are for the descending excitation power. (b) Zoom-in

plot from the dashed box in (a). At the highest laser powers (12.9 mW), we observe a clear, reversible blue-shift of the out-of-plane mode (A_{1g}). Since the Raman spectral changes are reversible with lower laser power, we conclude that the A_{1g} shift is solely related to the temperature increase during illumination, and the effects are not permanent. Based on the A_{1g} blue-shift and the reported temperature-A_{1g} coefficients (-0.0121 and -0.0149 cm^{-1}/K), we estimate the local temperature at the highest excitation power (12.9 mW) is about 223 – 270 C. [3,4] Since the WS_2 has been annealed in N_2 at 300 °C before the in-situ PL measurement, the PL changes are not likely due to the laser introduced heating.

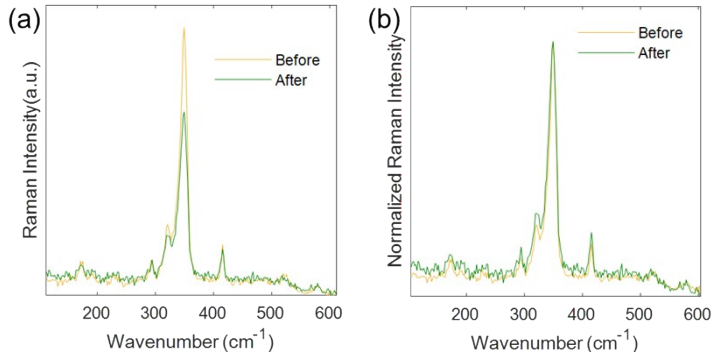

Figure S8. Raman spectra of the WS_2 flake in an N_2 environment before and after 1000 s, where (a) is the raw data, and (b) is the normalized data. The 532-nm laser power is 889 μW.

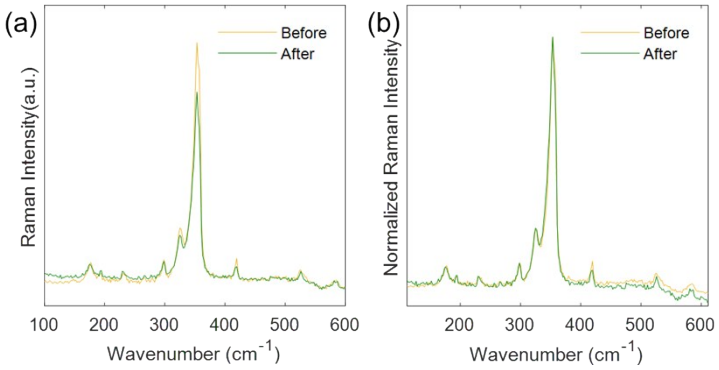

Figure S9. Raman spectra of the WS_2 flake in O_2 before and after 1000 s, where (a) is the raw data, and (b) is the normalized data. The 532-nm laser power is 889 μW.

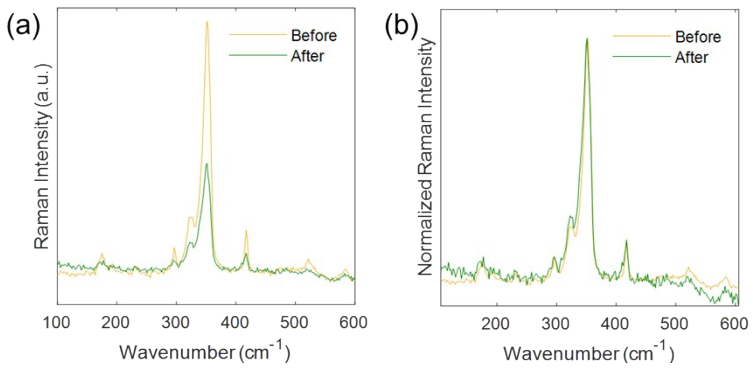

Figure S10. Raman spectra of the WS_2 flake in H_2O vapor before and after 1000 s, where (a) is the raw data, and (b) is the normalized data. The 532-nm laser power is 889 μW.

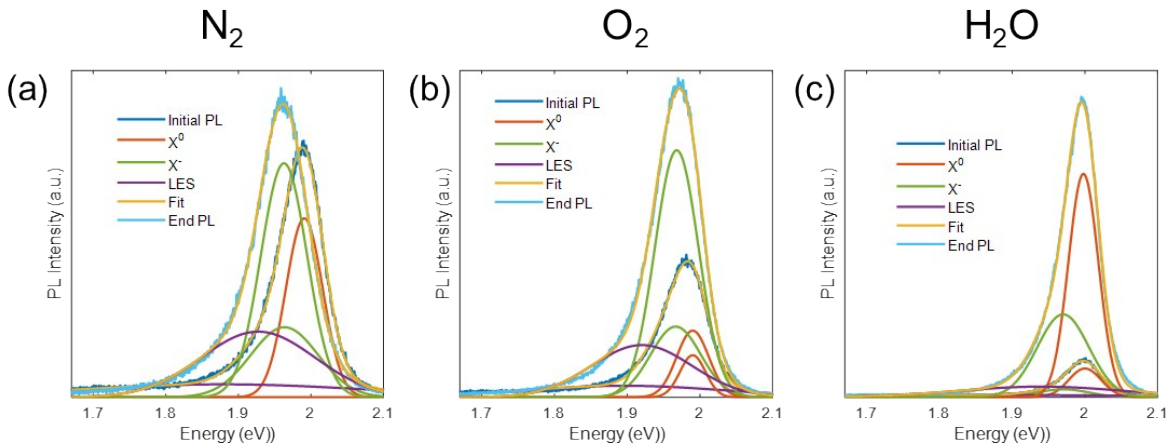

Figure S11. PL intensity of monolayer WS_2 before (light blue) and after (blue) ~1000 s of continuous 532-nm laser illumination in (a) N_2, (b) O_2, and (c) H_2O, respectively, along with three Gaussian components (X^0 – red, X^- – green, LES – purple) and the overall fitting results (yellow).

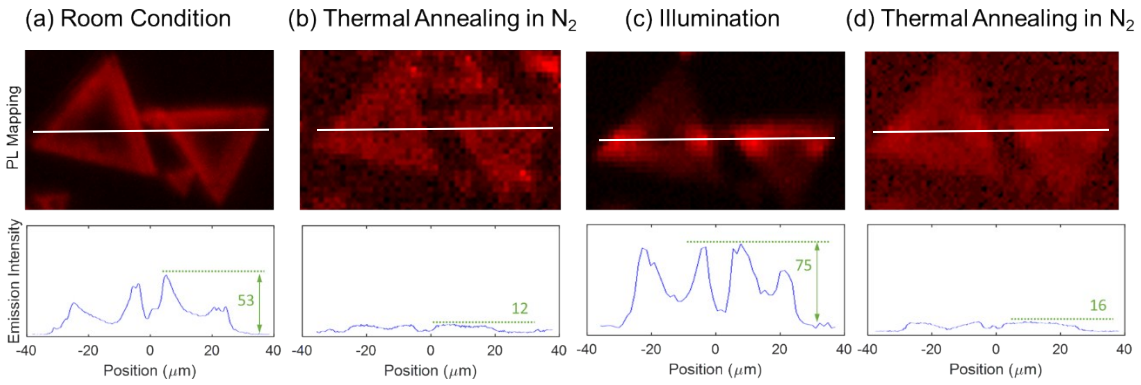

Figure S12. Upper panel: PL intensity mapping reconstructed at 630 nm or 1.968 eV. Lower panel: PL intensity line profiles of the PL intensity maps reconstructed at 630 nm or 1.968 eV. (a) PL mapping measured under ambient room conditions. (b) PL mapping for the WS_2 sample thermally annealed in N_2 at 300 °C for 1 hour. (c) PL mapping after excess 532-nm laser irradiation at the centerline of WS_2 in O_2. (d) PL mapping of the WS_2 after thermal annealing in N_2. The excitation laser intensity is 119 μW with 1 s integration time and one accumulation.

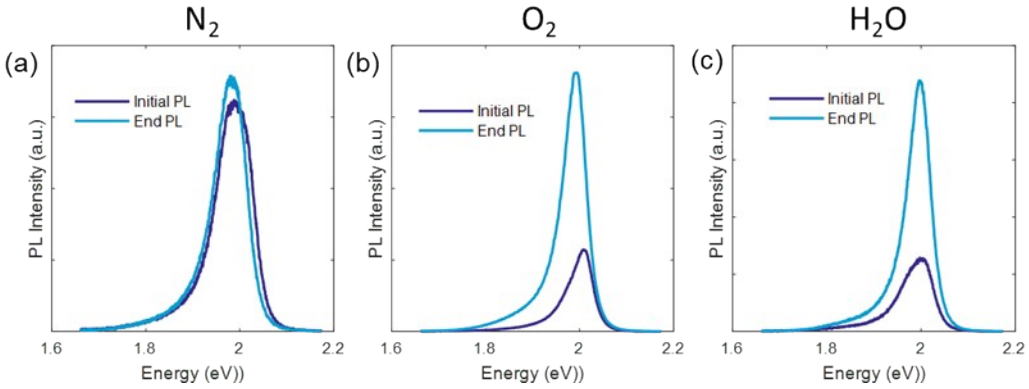

Figure S13. PL changes for alternative CVD growth condition (sulfur deficient conditions[5]) of WS_2 flake in (a) N_2, (b) O_2, and (c) H_2O environments. The overall trend for the new, sulfur deficient sample is very similar to the original sample (highlighted in the main text), including the same intensity before and after laser irradiation in N_2 with a slight redshift, the enhanced PL in O_2 with a red-shifted peak, and increased PL in H_2O with a slightly blue-shifted peak. One different distinguishing feature of the sulfur deficient sample is, in the H_2O environment, PL is enhanced only about ~3 instead of ~7 for the original sample in the manuscript. This might be due to the different defect density for different CVD growth techniques.

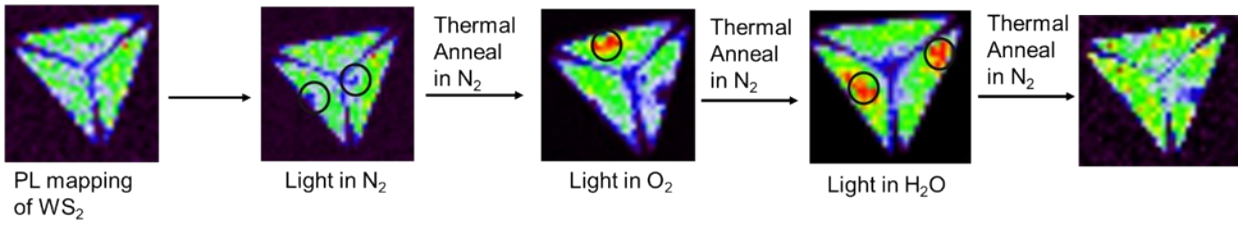

Figure S14. Additional PL mapping experiments showing the reversibility of the PL enhancement of one sulfur deficient CVD WS_2 flake, as described in Figure S13. The black circle indicates the irradiation spots. The thermal annealing in N_2 can recover the PL enhancement in the O_2 and H_2O with the laser irradiation, strongly suggesting the structure reversibility upon thermal annealing. The excitation laser is 532 nm with 119 μW. The PL mappings are reconstructed at 2 eV.

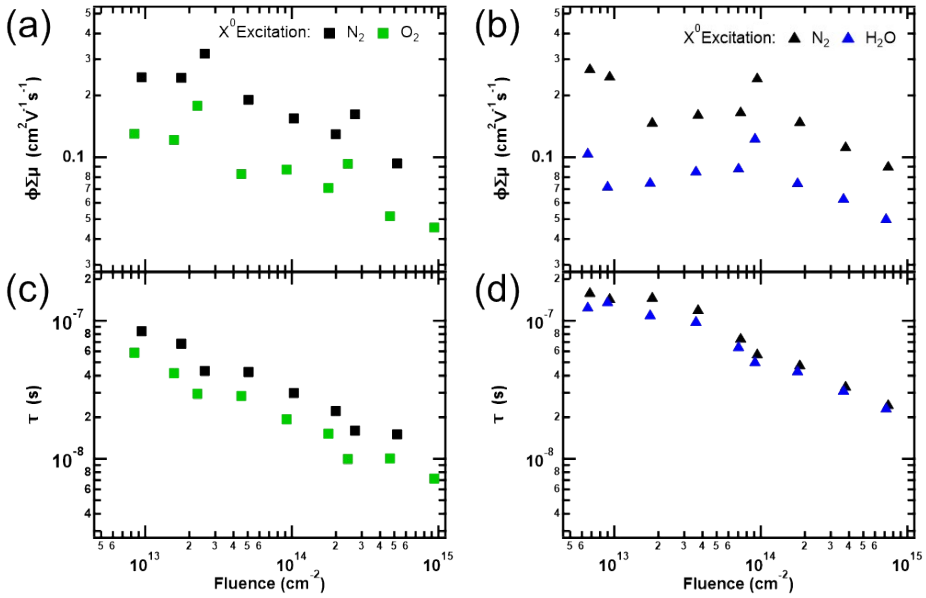

Figure S15. (a,b) Yield-mobility product and (c,d) amplitude-weighted average lifetime as a function of absorbed laser fluence of monolayer WS_2 on quartz. The photoexcitation wavelength is 2.02 eV. The samples are pre-treated as described in the main text; results are given for N_2 (black in a,b,c,d), O_2 (green in a,c), and H_2O (blue in b,d).

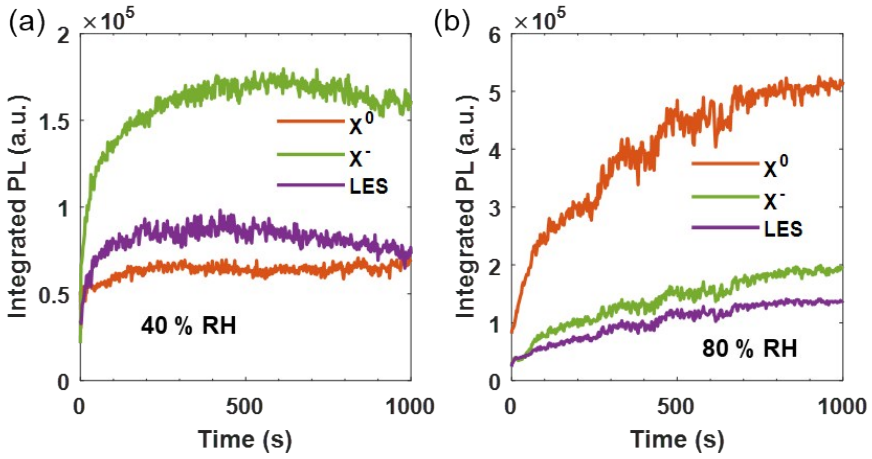

Figure S16. The decomposed PL Gaussian fitting results for the X^0, X^-, and LES contributions as a function of 1000-s laser irradiation in (a) 40% relative humidity and (b) 80% relative humidity.

References

(1) Kim, M. S.; Yun, S. J.; Lee, Y.; Seo, C.; Han, G. H.; Kim, K. K.; Lee, Y. H.; Kim, J. Biexciton Emission from Edges and Grain Boundaries of Triangular WS2 Monolayers. *ACS Nano* **2016**, *10* (2), 2399–2405. https://doi.org/10.1021/acsnano.5b07214.

(2) Shang, J.; Shen, X.; Cong, C.; Peimyoo, N.; Cao, B.; Eginligil, M.; Yu, T. Observation of Excitonic Fine Structure in a 2D Transition-Metal Dichalcogenide Semiconductor. **2015**, *9* (1), 9.

(3) Peimyoo, N.; Shang, J.; Yang, W.; Wang, Y.; Cong, C.; Yu, T. Thermal Conductivity Determination of Suspended Mono- and Bilayer WS2 by Raman Spectroscopy. *Nano Res.* **2015**, *8* (4), 1210–1221. https://doi.org/10.1007/s12274-014-0602-0.

(4) Huang, X.; Gao, Y.; Yang, T.; Ren, W.; Cheng, H.-M.; Lai, T. Quantitative Analysis of Temperature Dependence of Raman Shift of Monolayer WS 2. *Sci. Rep.* **2016**, *6* (1). https://doi.org/10.1038/srep32236.

(5) Blackburn, J. L.; Zhang, H.; Myers, A. R.; Dunklin, J. R.; Coffey, D. C.; Hirsch, R. N.; Vigil-Fowler, D.; Yun, S. J.; Cho, B. W.; Lee, Y. H.; et al. Measuring Photoexcited Free Charge Carriers in Mono- to Few-Layer Transition-Metal Dichalcogenides with Steady-State Microwave Conductivity. *J. Phys. Chem. Lett.* **2020**, *11* (1), 99–107. https://doi.org/10.1021/acs.jpclett.9b03117.